Cold-Formed Steel Examples to the Theory and Finite Element Implementation of Plasticity

Seventeenth International Specialty Conference on Cold-Formed Steel Structures
Orlando, Florida, U.S.A., November 4-5, 2004

Cold-Formed Steel Examples to the Theory and Finite Element Implementation of Plasticity

Dr. H.(Herm) Hofmeyer[1]

Abstract

This paper presents two examples to the theory and finite element implementation of plasticity. The first example is on the cross-sectional behavior of trapezoidal sheeting subjected to a concentrated load. It is shown that the number of elements (and thus the number of integration points) along the corner radius are important for the correct modeling of this static problem. The second example is on the failure of first-generation sheeting subjected to a concentrated load and a bending moment. This problem, especially for large span lengths, can be solved only with explicit dynamic simulations. These are, for our research field, for the first time published here. The explicit simulations normally function with a rather simple integration scheme for plasticity; is shown that our sheeting results are very sensitive to this.

Introduction

In a previous paper [Hofm04a], an introduction to the theory and finite element implementation of (steel) plasticity was given. In this paper two examples will be presented. The first example is on the cross-sectional behavior of trapezoidal sheeting subjected to a concentrated load. The second example is on the failure of first-generation sheeting subjected to a concentrated load and a bending moment. Both examples show which problems can be avoided if number of elements and integration schemes for plasticity are chosen correctly. The second example shows that for long spans, it can be solved only with explicit dynamic simulations. These are, for our research field, for the first time published here. Both examples are presented by explaining background information and finite element model setup (1), a parameter study (2), and conclusions (3).

[1] Assistant professor Applied Mechanics, Technische Universiteit Eindhoven, The Netherlands and specialist-project manager ABT consulting engineers, Arnhem, The Netherlands

1 Cross-sectional behavior of trapezoidal sheeting

1.1 Background information and finite element model setup

For short three-point bending tests on trapezoidal sheeting, after elastic behaviour, the rolling post-failure mode behaves plastically and increases in strength. After further deformation, the strength reduces. The yield-arc post-failure mode decreases in strength immediately after elastic behaviour. A rolling post-failure mode starts with two moving yield lines near the upper corner. With increasing load, the moving yield line in the web moves downwards in the web. The moving yield line in the top flange moves through the corner. A yield-arc post-failure mode starts with a curved yield line in the web. With increasing load, this yield line is practically fixed.

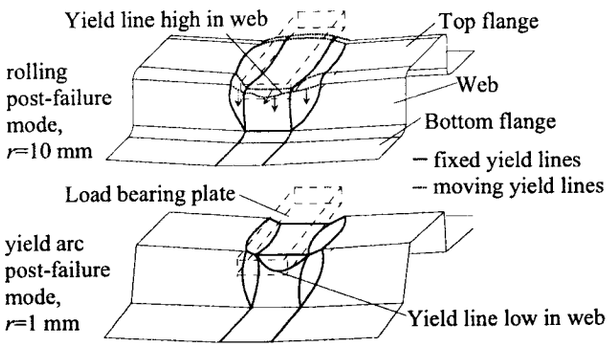

Figure 1, post-failure modes for experiments: three-point bending tests.

Bakker introduced simple mechanical models for the rolling and yield-arc post-failure modes [Bakk96a]. The simple post-failure models suggest that if differences between the two post-failure modes are investigated, it is sufficient to investigate the sheeting's cross-section only. The investigation of differences between the two post failure modes will be carried out by a finite element model.

For the finite element model, a strip of the section's cross-section is loaded by a load bearing plate, which is modelled as a solid piece of steel. The strip is loaded by a forced displacement of the load bearing plate. Contact elements are modelled between the load bearing plate and the top flange of the strip to

prevent penetration of the load bearing plate into the strip. Because of symmetry conditions, the strip width does not influence the results. The strip width of the model is chosen arbitrarily to be dx=3 mm. Element sizes are 3*3 mm for web and top flange. The corner has a radius r and is modelled by 10 elements over the corner circumference. Shell elements are used, having four nodes with six degrees of freedom each.

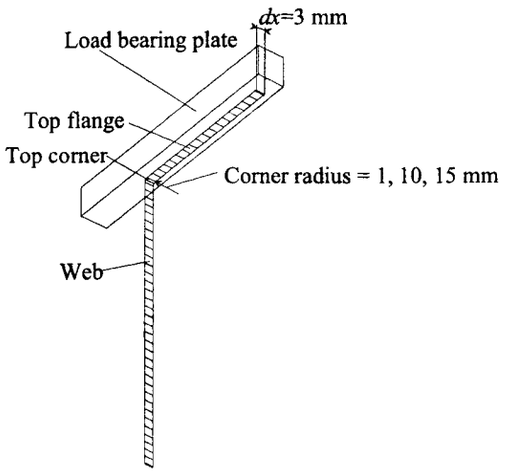

Figure 2, finite element model of strip.

If load deformation curves of the strips (cross-section, numerical) and curves for normal sheeting (total section, experimental) are compared, it can be seen that for r=1 the load-deformation behaviour are qualitative similar. For r=10, the curves are qualitatively different: whole hat-sections show an ascending plastic curve after plastic mechanism initiation and hereafter a descending plastic curve. Strips show a descending plastic curve directly after elastic behaviour for all corner radii.

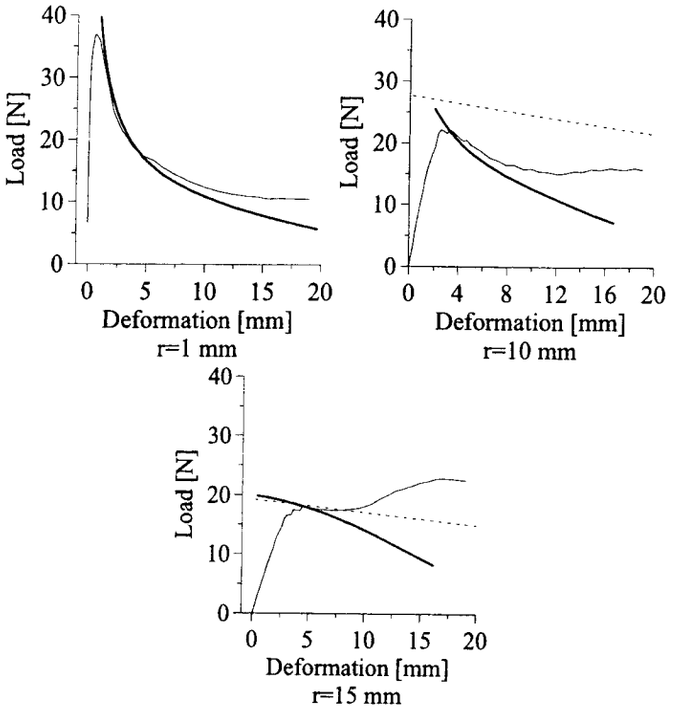

Figure 3, different corner radii: the normal line presents the finite element simulation (bold and dotted lines are theory).

For a strip, for all corner radii, first a yield line will occur in the web. The position of this yield line depends on the corner radius. During further deformation, this yield line will move downwards in the web. Again this movement depends on the corner radius. Hereafter, yield lines will occur in the top flange and at the bottom of the strip. For r=15 mm, an additional yield line occurs in the top corner.

For small corner radii, the location, and movement of yield lines in the strips are quite similar to the yield lines of the finite element model for a whole hat-section. For large corner radii, this is not the case: for a whole hat-section, two moving yield lines occur near the top corner (a rolling post-failure mode), whereas for the strip only one yield line in the web occurs. For a strip with a

corner radius r=15 mm, after some deformation, an additional yield line did occur in the corner radius: this looks like a rolling mechanism.

1.2 Parameter study

For the model, four-node shell elements (Ansys SHELL43) were used, having extra displacement shapes. The integration scheme is 2*2 along the surface and 5 integration points along the thickness, because non-linear material behaviour is present. The mesh density along the corner radius was varied as shown in figure 4. Using the default integration scheme of the four node shell elements, this thus alters the amount of integration points along the corner radius.

For a small corner radius (r= 1 mm) it is known that the yield lines occurring in web and flange do not move [Bakk96a]. Figure 4 shows that using one, two, or three elements does not alter the results, even far beyond the ultimate load, in the plastic phase. The section is deformed so strongly then, that other elements in the corner radius contact the load bearing plate. However, also this effect does not seem to affect the results. For a large corner radius (r= 10 mm), 20 elements predict the behaviour smooth and well (see also figure 3). For less elements, it is clear that the load deformation curve quality is affected.

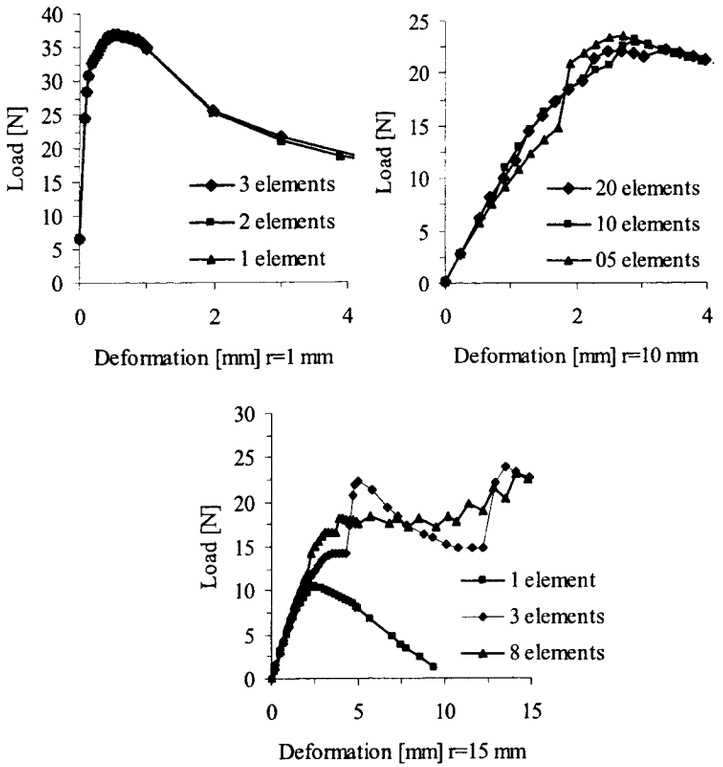

Figure 4, numerical simulations with r = 1, 10, and 15 mm with different elements along the corner radii.

For five elements, linear elastic behaviour immediately changes into plastic behaviour without convergence in between. After plasticity has taken place seriously, curves converge to one solution. This means that for this amount of plastic yield line movement, the amount of integration points is still not critical in the phase after ultimate load.

For a corner radius equal to 15 mm, behaviour for 8 elements already shows oscillating results, clearly due to the yield line running trough the integration points. The model having 3 elements yields unusable results. The model with 1 element shows surprisingly smooth results, but this because in fact a different geometry is simulated. Plastic capacity after ultimate load is predicted too low.

1.3 Conclusions

For cross-section behaviour, the number of integration points is not relevant for simulations with a small corner radius (no moving yield lines). For large corner radii (10 mm), moving yield lines occur and prediction of the behaviour around the ultimate load is sensitive to the number of integration points. However, plastic behaviour for large deformations is not sensitive to the number. For very large corner radii (> 15 mm) the ultimate load and post-critical plastic behaviour are not predicted well for a small number of integration points. As a conclusion, the number of integration points is of importance for the prediction of the ultimate load for large radii, and for the prediction of ultimate load and post-critical behaviour for very large radii.

2 Failure of first-generation sheeting subjected to a concentrated load and a bending moment

2.1 Background information

Normal to large span first-generation sheeting fails by the rolling and yield arc post-failure modes (figure 6) but normally via the yield eye post-failure mode. The yield eye post-failure mode resembles the yield arc post-failure mode, but is asymmetric in length direction (figure 6). In a thesis [Hofm00a], finite element models were presented to simulate the rolling, yield arc and yield eye post-failure modes. It was explained that the finite element model for the yield eye post-failure mode could not use a load-bearing plate and contact elements to model the load application. To qualitatively investigate why this is the case, a spring model was developed, as shown in figure 5. This spring model was made using a finite element program.
With the spring model, a sheet section three point bending test can be modeled. The triangles of rigid beams on the left and right of the model are very stiff; they model the parts of the sheet section that do not deform. At the bottom of the model, three rigid beams and four hinges are included. These parts model the bottom flange of the sheet section. The linear springs are a very simple way to model the cross-sectional stiffness of the sheet section. Note that although the figure suggests differently, the springs are only capable of introducing forces in y-direction and not in x-direction in the finite element program.

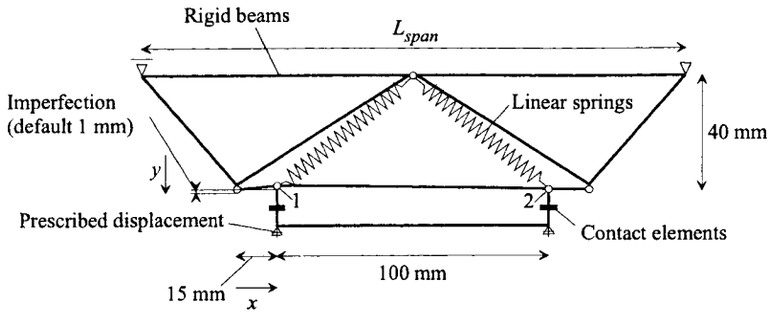

Figure 5, spring model.

Load is applied by an equal prescribed displacement to the left and right sides of a rigid beam. This beam enforces displacement on the spring model, but only if there is compression in the contact elements (a displacement of the rigid beam in positive y-direction will not result in loading of the spring model). The length L_{span} is a variable. The spring stiffness equals 100 N/mm. An initial imperfection is applied by slightly raising the left hinge below the left spring in negative y-direction. The default imperfection is 1 mm. A geometrically non-linear calculation is made: the Newton-Raphson method is used. The maximum displacement is limited to stop the calculation.

For the experiments in the thesis [Hofm00a], there was a tendency for the asymmetric yield eye post-failure mode to occur for experiments with a large span length (2400 mm), while the symmetric yield arc post-failure mode occurred for experiments with a small span length (600 mm). The span length was varied for the spring model. Six values were taken: 400, 800, 1200, 1600, 2000, and 2400 mm. Table 1 presents the results. For small lengths a symmetric post-failure mode did indeed occur and for large lengths an asymmetric post-failure mode did occur (figure 6). Thus, this simple spring model traces the difference between these two post-failure modes.

Table 1, post-failure modes and other data for varying span length.

Span length [mm]	Post-failure mode	Convergence	Ultimate load [N]
400	Symm. (yield arc).	Yes.	162
800	Symm. (yield arc).	Yes.	101
1200	Symm. (yield arc).	Yes, but not far after ultimate load.	75
1600	Not known.	No.	Not known.
2000	Asym. (yield eye).	Yes.	48
2400	Asym. (yield eye).	Yes.	41

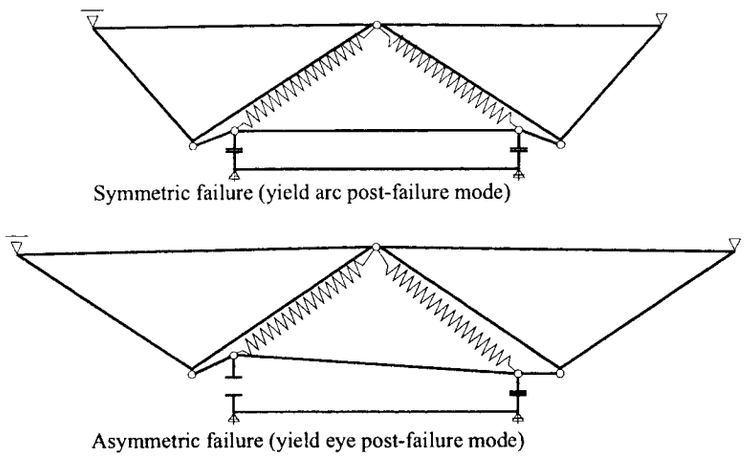

Figure 6, two different post-failure modes for simple spring model.

The ultimate load is plotted against the span length in figure 7 on the left. Although only a few data points are available, the figure on the left suggests that there is one curve for the yield arc and yield eye post-failure modes. In other words, a change in post-failure mode does not have consequences for the ultimate load.

To see whether the change from a symmetric into an asymmetric post-failure mode is gradual or instant, the difference in displacement of point 1 and 2 (figure 5) is recorded versus the load. Figure 7 shows this on the right. Displacement differences for span length 2000 mm and 2400 mm are maximally

2.25 mm. This is not shown in the figure, because the scale of the *x*-axis is limited. The scale is limited to give an idea about the displacement differences for other span lengths. It is clear that there is no gradual behavior of the displacement differences. This means that the transition from a symmetric to an asymmetric post-failure mode is an instant transition. This could also mean that convergence problems occur at or near this instant transition. This is what probably happened for a span length of 1600 mm, table 1.

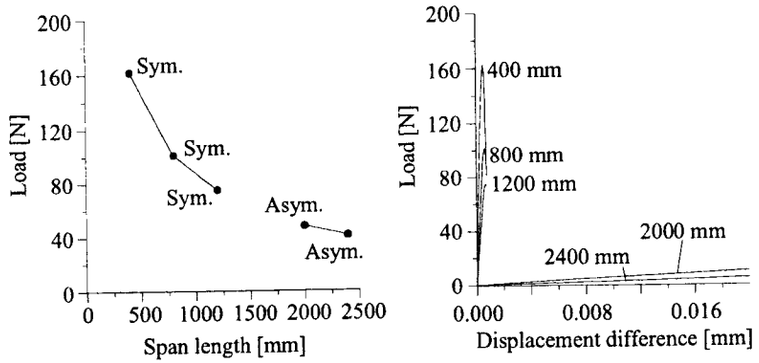

Figure 7, ultimate load and displacement differences for different span lengths (spring model).

In the thesis it is mentioned that yield arc and yield eye post-failure modes show the same behavior and are both symmetric at ultimate load. Only after ultimate load are there differences. The yield arc post-failure mode remains symmetric. However, the yield eye post-failure mode changes from symmetric into asymmetric. The spring model showed that there is an instant transition between symmetric and asymmetric behavior. Thus, after the ultimate load, such an instant transition arises for the yield eye post-failure mode. At this instant transition, the load-bearing plate contact changes instantaneously from the whole load-bearing plate to one edge of it. A possible reason for no convergence of the finite element model is that the contact elements and the solution algorithm cannot follow the quick contact changes. Therefore, simulations have been made using an explicit dynamic approach, using the program LS-DYNA [Rust03a]. The advantage of using an explicit dynamic approach is that sudden contact changes do not create a problem, because convergence is not necessary. The program derives displacements by integrating speed and speed by integrating accelerations. These accelerations are found by the forces applied in

time on the specific masses. A disadvantage is that small steps in time have to be taken to avoid stress waves traveling through more than one element. To simulate a static situation, as for our case, simulation time has to be long enough to avoid dynamic effects. However, small steps have to be taken, thus giving the need to find a balance between avoiding dynamic effects and a short enough simulation time. Furthermore, the LS-DYNA shell elements use a very simple integration schema as default. This works fine for highly dynamic simulations like car-crashes, but is it suitable for our quasi-static sheeting problem?

2.2 Finite element model and parameter study

Figure 8 shows the finite element model. Test h61 [Hofm00a] was taken. This test has a span length of 2400 mm, web height 100 mm, compressed flange width 40 mm, corner radius 5.8 mm, angle between web and flange 44 degrees, steel thickness 0.61 mm. The geometry was defined by defining the cross-section by the corners and the corner radius for the compressed flange by the two outer points. The geometry was swept over the section length. A half model was needed to model the asymmetrical yield eye post-failure mode. Elements used were four node shell elements SHELL163, 12 degrees of freedom for each node (3 displacements, 3 rotations, 3 velocities, 3 accelerations). The elements are numerically integrated by 2 points along the thickness and 1 point on the surface. For the meshing, note that along the corner radius adjacent to the compressed flange, one element along the cross-section is used. This is sufficient, see chapter 1 of this paper. For the material, the real stress-strain curve is used.

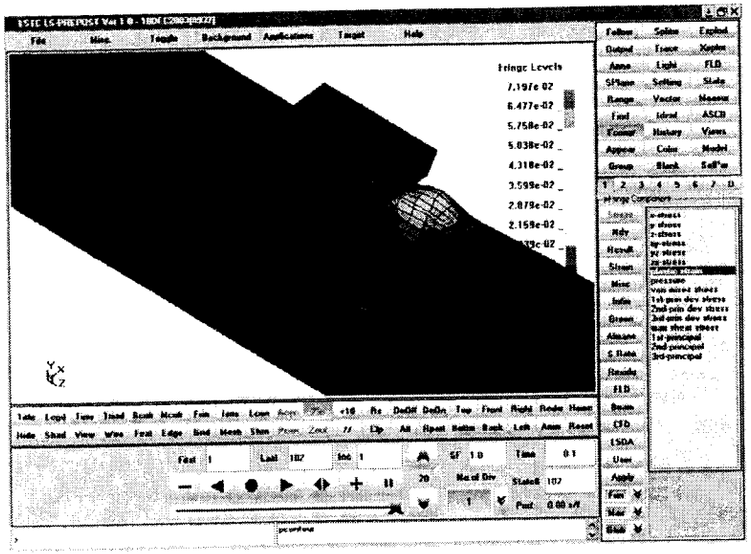

Figure 8, LS-DYNA finite element model, roof post-failure mode.

The load is applied by a load bearing plate, the plate is modeled as a rigid body. The rigid body is lightly wedge shaped to prevent erroneous contact resulting in "spikes"; nodes that are pushed away aggressively by the contact algorithm. Total simulation times equals 100 ms, the speed in negative *y*-direction of the rigid body starts with 0 and ends with 600 m/s, thus the end *y*-displacement of the rigid body equals -30 mm.

The symmetry line has appropriate boundary conditions: *x*-displacements, and *y*- and *z*-rotations are zero. Along the edge of the flange under tension, *x*-displacements are zero, thus simulating full sheeting or strips preventing spreading of the webs. The supports are modeled by preventing *z*-displacements along a line perpendicular to the length of the flange tensioned.

Table 2 presents the variations of the model with regards to the number of integration points and their location.

Table 2, parameter study for post-failure modes and other data for varying span length.

Simulation	Number of integration points and their location	Failure mode	Ultimate load [N]
h61	Surface: 1, 2 along thickness	Roof [Mahe97a]	1656
h61_bt	Surface: 2*2, 2 along thickness	Undefined	Unusable
h61_3p	Surface: 1, 3 along thickness	Yield arc [Hofm00a]	1622
h61_5p	Surface: 1, 5 along thickness	Yield arc [Hofm00a]	1620
h61_3p_30	Surface: 1, 3 along thickness, bearing plate eccentricity 30 mm.	Yield eye [Hofm00a]	1631

2.3 Conclusions

The results concerning the failure mode in table 2 show that the simulations are very sensitive to the plastic behavior of the element. However, the ultimate load is stable for the different solutions. If the understanding of the failure mode has priority, the plastic behavior of the element should be carefully chosen. The previous paper [Hofm04a] explains the principles of plastic behavior and can be used for this. The table shows that to force the yield eye post-failure mode to occur, a serious imperfection has to be used. The load bearing plate has shifted to the right over 30 mm! Future research will focus on a sensitivity study for which values the yield arc and for which values the yield eye post-failure mode will occur.

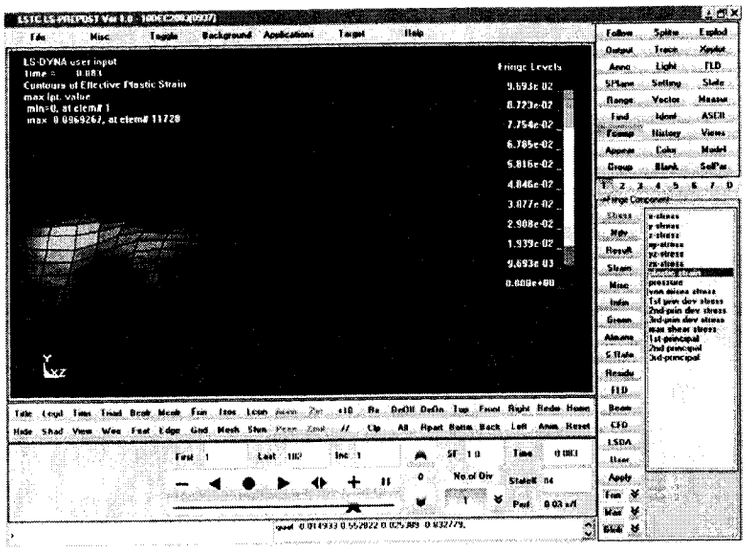

Figure 9, LS-DYNA finite element model, yield eye post-failure mode.

3 Conclusions

For cross-sectional behaviour with moving yield lines, the number of integration points is not of importance for small radii. It is of importance for the prediction of the ultimate load for large radii, and for the prediction of ultimate load and post-critical behaviour for very large radii.

For explicit dynamic simulations, the simulations are very sensitive to the plastic behavior of the element. If the understanding of the failure mode has priority, the plastic behavior of the element should be carefully chosen. The previous paper [Hofm04a] explains the principles of plastic behavior and can be used for this.

To force the yield eye post-failure mode to occur, a serious imperfection has to be used. Future research will investigate under which circumstances the yield arc and for which circumstances the yield eye post-failure mode will occur.

References

[Bakk92a] Bakker, M.C.M., Web crippling of cold-formed steel sections, Dissertation Eindhoven University of Technology, The Netherlands, 1992.

[Hofm00a] Hofmeyer, H.: Combined Web Crippling and Bending Moment Failure of First-Generation Trapezoidal Steel Sheeting, Ph.D.-thesis, Eindhoven University of Technology, Faculty of Architecture, Department of Structural Design, ISBN 90-6814-114-7, The Netherlands, 2000.

[Hofm04a] Hofmeyer, H.: Introduction to the Theory and Finite Element Implementation of (Steel) Plasticity, to be presented at the 17th International Speciality Conference Cold-Formed Steel Structures, November 4 & 5, 2004, Orlando, Florida, U.S.A.

[Mahe97a] Mahendran, M.: Local plastic mechanisms in thin steel plates under in-plane compression, Thin-Walled Structures, Volume 27, Issue 3, March 1997, Pages 245-261.

[Rust03a] Rust, W.; Schweizerhof, K.: Finite element limit load analysis of thin-walled structures by ANSYS (implicit), LS-DYNA (explicit) and in combination, Thin-Walled Structures, Volume 41, Issues 2-3 , February 2003, Pages 227-244.

[Timo36a] Timoshenko, S., Theory of Elastic Stability, Engineering Societies Monographs, McGraw-Hill Book Company, New York and London, First edition, 1936.